International Symposium
On Turbulence and Shear Flow
Phenomena (TSFP-9)
June 30 - July 3, 2015 *Melbourne, Australia*

PRELIMINARY ANALYSIS OF PERMEABLE COATINGS FOR TURBULENT DRAG REDUCTION

Nabil Abderrahaman & Ricardo García-Mayoral
Department of Engineering
University of Cambridge
Trumpington St, Cambridge, CB2 1PZ, UK
r.gmayoral@eng.cam.ac.uk

ABSTRACT

This study focuses on permeable coatings as a form of passive flow control. A simplified model is proposed to analyse the qualitative effect of the coating's thickness and permeability on drag reduction. For small permeability, the reduction is linear with the length scale of the streamwise permeability. For larger permeability, a degradation mechanism is investigated that depends critically on the geometric mean of the streamwise and wall-normal permeabilities. For a streamwise-to-wall-normal permeability ratio of order 10-100 the maximum drag reduction is predicted to be 15-25%.

INTRODUCTION

Various surface geometry manipulations have been studied as forms of passive flow control to reduce viscous drag in turbulent flows, and a few of them have been shown to achieve this goal. For instance, surface riblets (Walsh & Lindemann, 1984) and superhydrophobic surfaces (Rothstein, 2009) are techniques that have demonstrated to reduce friction.

In this work, we study the use of anisotropically-porous media to reduce turbulent skin friction. Hahn *et al.* (2002) showed that, in channel flows, friction can be reduced by means of substrates permeable only in the streamwise direction. These surfaces can create an apparent slip on the overlying turbulent flow. Since the permeability is anisotropic, the effective slip depends on the orientation with respect to the flow. This is analogous to the drag-reducing effect of riblets, which hinder the spanwise motions while favouring the streamwise ones, creating an apparent slip for the overlying flow.

The studies of Luchini *et al.* (1991) and Jiménez (1994) establish a relationship between the slip and the skin friction, and also predict that the slip length is proportional to the length scale of surface manipulations. However the linear-with-size behaviour begins to deteriorate beyond a certain size, as observed by García-Mayoral & Jiménez (2011*b*) for riblets. They showed that the physical mechanism producing this degradation was the appearance of spanwise rollers produced by a Kelvin-Helmholtz instability. These instabilities have also been found over several different surfaces, such as plant canopies (Finnigan, 2000; Py *et al.*, 2006), and porous surfaces (Jiménez *et al.*, 2001; Breugem *et al.*, 2006). In the case of permeable substrates, Jiménez *et al.* (2001) found that this instability can be triggered by wall-normal permeability alone.

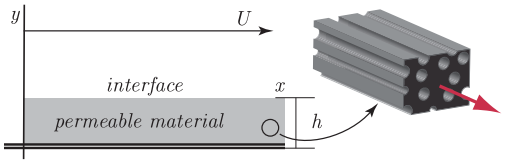

Figure 1. Schematic representation of an anisotropic permeable layer for drag reduction.

The present work assesses the potential capacity of permeable media to produce drag reduction in turbulent flows. We consider an anisotropically-permeable layer, as depicted in figure 1. It is characterised by its thickness, h and its streamwise, spanwise and wall-normal permeabilities, K_x, K_z and K_y, which are assumed to be along the principal directions of the permeability tensor K. To maximise the effect of Hahn *et al.* (2002) and to minimise the drag-increasing one of Jiménez *et al.* (2001), we consider in principle coatings with high K_x and low K_y.

DRAG REDUCTION BY A POROUS INTERFACE

While for conventional smooth walls the velocity is zero at the wall, surface manipulations may produce a non-zero velocity at a notional wall plane. These slip velocities have been shown to reduce skin friction in certain cases (Luchini *et al.*, 1991; Jiménez, 1994). Here we investigate the possibility of producing such slip by using porous coatings.

Slip and skin friction

The slip produced by surface manipulations results in a shift of the logarithmic layer, which is related to the variation in skin friction (Jiménez, 1994). The velocity profile in the logarithmic layer is

$$U^+ = \frac{1}{\kappa}\log y^+ + B, \qquad (1)$$

where B is the near-wall intercept. The superscript '+' indicates viscous-unit scaling. In the classical theory of wall turbulence, surface manipulations only modify the intercept of this logarithmic velocity profile, while both the Kármán

constant, $\kappa \approx 0.4$, and the wake function are unaffected (Nikuradse, 1933; Clauser, 1956). Hence, a permeable substrate is expected to affect the logarithmic profile by only producing changes in B, at least for small permeability. As shown by García-Mayoral & Jiménez (2011*a*), for a constant velocity and small changes of B and the friction coefficient, c_f, expression (1) leads to

$$DR = \frac{\Delta c_f}{c_{f_0}} \approx \frac{-\Delta B}{(2c_{f_0})^{-1/2} + (2k)^{-1}}, \tag{2}$$

where the '0' subscript indicates the reference value for a smooth-wall. If ΔB is positive, the logarithmic profile is shifted upwards and friction is reduced, and vice versa.

The work carried out by Jiménez (1994) established the relation between ΔB and the slip velocities. In the limit of vanishingly small surface manipulations, the shift of the logarithmic profile is proportional to the difference between the longitudinal and transverse slip velocities

$$\Delta B = \mu_0 \ell_s^+ = \mu_0 (\ell_x^+ - \ell_z^+), \tag{3}$$

where $\mu_0 \approx 0.66 - 0.785$ is a universal constant (García-Mayoral & Jiménez, 2011*a*; Bechert *et al.*, 1997). Intuitively, if the cross-flow is more impeded than the streamwise one, the streamwise vortices are pushed away from the wall. This reduces the turbulent momentum exchange with high velocity layers farther away from the wall, and skin friction is eventually reduced.

For typical values of c_{f_0} in flows at $Re_\tau \approx 1000 - 10000$, the drag reduction is then

$$DR \approx \frac{\Delta c_f}{c_{f_0}} \approx \frac{-\mu_0}{(2c_{f_0})^{-1/2} + (2k)^{-1}} \ell_s^+ \approx 0.05\, \ell_s^+. \tag{4}$$

Note that expression (4) is valid only for low values of ℓ_s^+. For high values, equation (3) would cease to hold as other mechanisms set in.

Slip-length by porous media

In order to estimate ℓ_x^+ and ℓ_z^+, the flow within the porous layer in response to the outer shear needs to be solved. Since in the viscous sublayer viscous effects are dominant, the mean velocity profile is linear. Therefore, the outer flow can be represented as a time-dependant, but otherwise uniform shear. Within the permeable substrate, we consider the streamwise momentum equation in a porous medium (Darcy, 1856; Brinkman, 1947),

$$\hat{\nu} \frac{\partial^2 u}{\partial y^2} - \frac{\nu}{K_x} u - \frac{\partial p}{\partial x} = 0, \tag{5}$$

where ν is the viscosity of the flow within the substrate, and $\hat{\nu}$ its apparent large-scale viscosity (Brinkman, 1947; Taylor, 1971; Ochoa-Tapia & Whitaker, 1995). Following Neale & Nader (1974), we assume that $\hat{\nu} \approx \nu$. As we are considering the flow driven by the overlying shear alone, the pressure terms in (5) can be neglected, resulting in a streamwise slip

$$\ell_x^+ \approx \sqrt{K_x^+} \tanh\left(\frac{h^+}{\sqrt{K_x^+}}\right). \tag{6}$$

An analogous expression can similarly be derived for the spanwise slip,

$$\ell_z^+ \approx \sqrt{K_z^+} \tanh\left(\frac{h^+}{\sqrt{K_z^+}}\right). \tag{7}$$

In the limit $h^+ \ll 1$, $\ell_s^+ = \ell_x^+ - \ell_z^+ \approx 0$. Since we are interested in obtaining values of ℓ_s^+ as large as possible, we focus on the opposite limit. For the same reason, we are also interested in $K_x^+ > K_z^+$. Under these conditions, $\ell_s^+ \approx \sqrt{K_x^+} - \sqrt{K_z^+}$, and expression (4) becomes

$$DR \approx 0.05 \left(\sqrt{K_x^+} - \sqrt{K_z^+}\right). \tag{8}$$

LIMIT FOR DRAG REDUCTION

The previous result supports the study carried out by Hahn *et al.* (2002), in which skin friction is reduced as streamwise permeability increases, thereby increasing ℓ_s^+. Note that equation (2) does not present any kind of limitation, so it would predict that drag would keep decreasing as ℓ_s^+ increases. However, Itoh *et al.* (2006) found that seal fur, which can be seen as a permeable material with x-preferential permeability, attains a maximum drag reduction at a certain ℓ_s^+, beyond which the drag reduction degrades in a fashion closely resembling that of riblets. In the case of riblets, beyond a certain size Kelvin-Helmholtz-like spanwise rollers develop over the surface, degrading the drag reduction effect (García-Mayoral & Jiménez, 2011*b*). Similar spanwise rollers have been observed over a variety of obstructed surfaces (Finnigan, 2000; Py *et al.*, 2006; Ghisalberti, 2009), including flows over permeable walls (Jiménez *et al.*, 2001; Breugem *et al.*, 2006), and have in general been found to be produced by a Kelvin-Helmholtz instability. It is therefore plausible to expect a similar mechanism taking place over anisotropic porous layers for certain values of their characteristic parameters. Jiménez *et al.* (2001) reported the appearance of spanwise rollers over surfaces permeable only in the wall-normal direction. This suggests that the wall-normal permeability may be key in the development of Kelvin-Helmholtz rollers, which would explain why they do not appear in Hahn *et al.* (2002). It also suggests that two competing mechanisms determine the change in drag, one beneficial and driven by the streamwise permeability, and one deleterious and driven by the wall-normal permeability.

Model from Linear Instability

The appearance of Kelvin-Helmholtz rollers over complex surfaces has previously been predicted successfully by linear inviscid stability analysis (Jiménez *et al.*, 2001; Py *et al.*, 2006; García-Mayoral & Jiménez, 2011*b*). Outside the porous layer, using the linearised perturbation equation for an inviscid flow, and searching for solutions of the form $f = \hat{f} \exp[i(\alpha_x x + \alpha_z z - \omega t)]$, Rayleigh's equation can be easily obtained (Schmid & Henningson, 2001)

$$(U - c)(\partial_{yy} - k^2)\hat{v} - U''\hat{v} = 0, \tag{9}$$

where U is the base flow, v the wall-normal perturbation velocity, α_x and α_z the wavelengths in streamwise and spanwise directions, $k^2 = \alpha_x^2 + \alpha_z^2$, ω the complex frequency, c

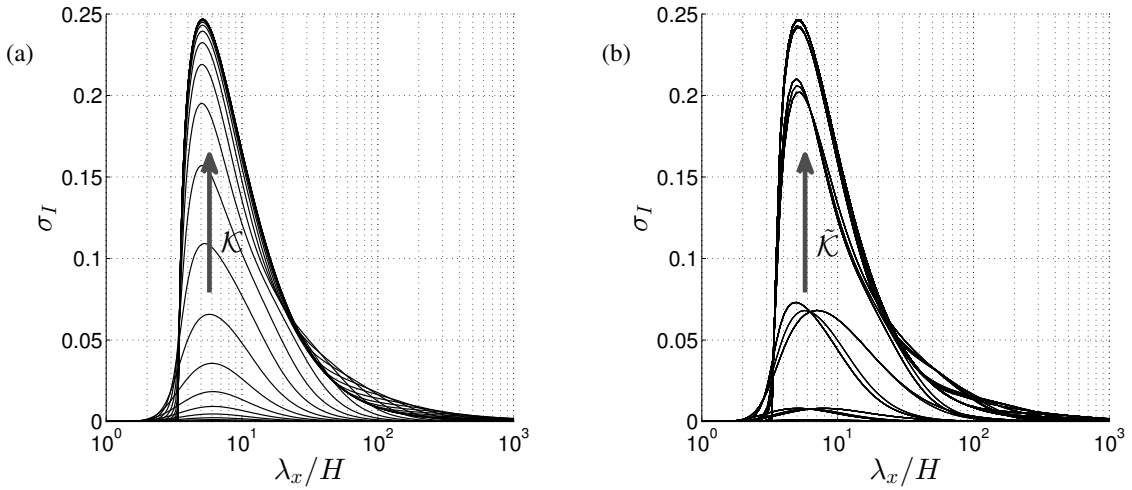

Figure 2. Growth rate $\sigma_I = Im(\sigma)$ of the unstable modes given by (12). (a) Isotropic case with $\Phi_{xy} = 1$ and $h/H = 1$ Curves are shown for values of $(\sqrt{K_x K_y}/H^2)(UH/\nu) = 10^{[-2(0.4)6]}$. (b) Anisotropic case obtained using all possible combinations of $h/H = 10^{[-1,0,1]}$ and $\Phi_{xy} = 10^{[-3(1)3]}$. Curves are shown for values of $\widetilde{\mathcal{K}} = 10^{[-2(1)6]}$.

the complex phase velocity defined as $\omega = \alpha_x c$, and where the prime superscript ($'$) indicates derivatives with respect to y.

Coupling with the porous layer

The difference between the present analysis and a smooth-wall case lies in the presence of the permeable coating, which imposes an impedance boundary condition on the outer flow (Jiménez *et al.*, 2001; Scalo *et al.*, 2014). To derive that boundary condition, we now focus on the response of the flow within the porous medium to outer pressure fluctuations. Let us consider the porous coating at the bottom wall, which extends from $-h$ to 0. The flow within the porous layer can be solved analytically to provide a boundary condition for the outer flow at $y = 0$. We also assume $h \gg \sqrt{K_x}$, since only deep-enough coatings produce a positive ℓ_s^+. As the overlying flow slips freely over the surface, there is no shear at the interface, and the Brinkman term is negligible. The flow within the permeable layer can then be simply described using Darcy's equation (Darcy, 1856); that is, equation (5) neglecting the first term. Defining Φ_{xy} as the anisotropy ratio $\Phi_{xy} = \sqrt{K_x/K_y}$, the resulting impedance condition is

$$\hat{v}_0 = -\widetilde{\alpha}\left[\frac{\sqrt{K_x K_y}}{\nu}\tanh(\widetilde{\alpha}\Phi_{xy}h)\right]\hat{p}_0, \qquad (10)$$

where $\widetilde{\alpha}^2 = \alpha_x^2 + \alpha_z^2 K_z/K_x$, and the subscript '0' stands for magnitudes at the interface.

Squire's transformation (Squire, 1933) reduces the problem to an equivalent one with $\alpha_z = 0$ and modified permeabilities. Oblique modes have lower permeabilities than their equivalent two-dimensional modes. As we will see below, this effect is stabilising. Consequently, we will only consider the case $\alpha_z = 0$, as it is the most unstable. This supports the idea that spanwise Kelvin-Helmholtz rollers are the most prevalent structures.

Results for a piecewise-linear profile

Before turning our attention to a more quantitative analysis, it is useful to study a piecewise-linear base flow

$$U(y) = \begin{cases} U_\infty y/H & \text{for } y < H, \\ U_\infty & \text{for } y \geq H, \end{cases} \qquad (11)$$

where the basic mechanisms are more easily understood. The advantages of this profile are that $U'' = 0$, and U' is constant, except where both U' and U'' present a jump discontinuity, at $y = H$. In combination with (9) and (10), this leads to a second order equation for the complex phase velocity c,

$$\begin{aligned} -2\mathcal{K}\sigma^2 + \left[-2i + \mathcal{K}\left(1 + 2\alpha' - e^{-2\alpha'}\right)\right]\sigma \\ + (\mathcal{K} - i)\left(1 - 2\alpha' - e^{-2\alpha'}\right) = 0, \end{aligned} \qquad (12)$$

where $\alpha' = \alpha H$, $\sigma = \alpha' c/U$ and

$$\mathcal{K} = \frac{\sqrt{K_x K_y}}{H^2}\left(\frac{U_\infty H}{\nu}\right)\tanh\left(\alpha'\frac{h}{H}\Phi_{xy}\right). \qquad (13)$$

Results of (12) as a function of $\mathcal{K}$ are shown in figure 2(a).

The limit $\mathcal{K} \gg 1$ provides a physical interpretation of the nature of the instability. In this limit, the boundary condition (10) is equivalent to $p(0) = 0$, which can be reduced to $\partial_y \hat{v}(0) = 0$. This gives the same solutions as extending the base profile antisymmetrically about $y = 0$, and enforcing symmetry on the perturbation flow. These solutions are the well-known Kelvin-Helmholtz unstable sinuous waves of a free shear layer, which are the only instabilities of the extended profile (Drazin & Reid, 1981). In the opposite limit, $\mathcal{K} \ll 1$, the neutral solution of a smooth impermeable channel is asymptotically approached. The intermediate values of $\mathcal{K}$ connect the Kelvin-Helmholtz solution with the stable one of the impermeable case.

Expression (13) depends not only on the porous coating properties but also on the spectral wavenumber, which is

not a physical property of the permeable layer. In an attempt to model this dependency in a simpler way we propose the following empirically fitted parameter

$$\widetilde{\mathcal{K}} = \frac{\sqrt{K_x K_y}}{H^2}\left(\frac{U_\infty H}{\nu}\right)\tanh\left(\frac{h}{H}\Phi_{xy}\right). \qquad (14)$$

Figure 2(b) portraits results as a function of $\widetilde{\mathcal{K}}$ for several combinations K_x, K_y and h. For the same values of $\widetilde{\mathcal{K}}$, solutions for different coatings collapse, except perhaps for low values of $\widetilde{\mathcal{K}}$, for which the instability is not fully developed. Other than for those low values, the empirical parameter $\widetilde{\mathcal{K}}$ encompasses the combined influence of the different coating properties.

It is worth pointing out that, while the amplification is determined by $\widetilde{\mathcal{K}}$, the lengthscale of the solution does not scale with the characteristic length of the porous material, $\sqrt{K_x}$ or $\sqrt{K_y}$. As in García-Mayoral & Jiménez (2011*b*), the lengthscale of the problem is determined by the height $y = H$ of the singularity in U'', that is, by the shape of the base flow.

Results for turbulent profiles

Although the analysis on the piecewise-linear velocity profile provides qualitative information on the nature of the instability, quantitative results for real applications require more realistic profiles. For that, we use the approximate turbulent mean profiles of Cess (1958). The stability problem (9), with the boundary condition (10), has now to be solved numerically.

For turbulent flows, the energy-producing term, U'', has a fairly sharp maximum between $y^+ = 5$ and 20, peaking near $y_c^+ = 8$, which plays the same role as the singularity at $y = H$ for the piecewise-linear profile. The peak scales in wall-units, and is responsible for the inner scaling of the instability, independently of Re_τ, as portrayed in figure 3 for the isotropic case. The solution is qualitatively similar to the one for the piece-wise linear profile, evolving from the neutral, smooth-wall solution to increasingly unstable solutions as the permeability increases, and eventually reaching a limit solution for high permeabilities.

The solution of the eigenvalue problem provides the characteristic wavelength of the instability, as well as the corresponding eigenmode. The perturbation velocity field of these unstable modes forms rollers turning alternatively clockwise and counter-clockwise. They have heights of $y^+ \approx 15$, and penetrate the porous material, below $y^+ = 0$, as illustrated in figure 4. As discussed above, this type of instability arises over many non-conventional surfaces in the form of spanwise rollers.

As in the case of the piecewise-linear mean velocity profile, we aim to describe the solution using a single characterising parameter. By analogy, we propose

$$\widetilde{K}^+ = \sqrt{K_x^+ K_y^+}\tanh\left(\frac{h^+}{y_c^+}\Phi_{xy}\right). \qquad (15)$$

Figure 5(a) illustrates how scaling with this parameter collapses all the solutions, as with the piecewise-linear profile. For high values of $\widetilde{K}^+$ the agreement is quite good, while for low values we can observe some scatter in the solution, depending on the value of $\Phi_{xy}h^+$. If the problem is linearly unstable, the most amplified mode will outstand

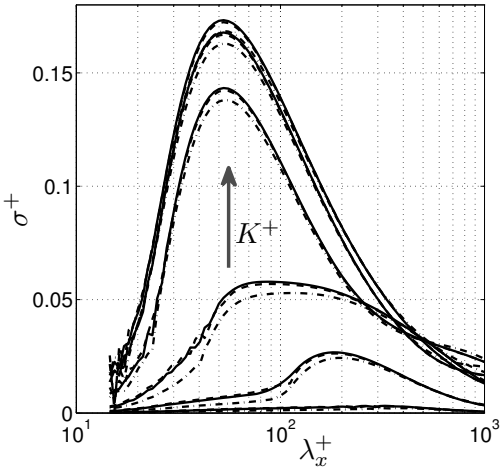

Figure 3. Growth rate $\sigma^+ = \alpha^+ Im(c^+)$ of the most amplified mode as a function of the longitudinal wavelength λ_x^+. Isotropic case, $K^+ = 10^{[-0.66(0.66)2.66]}$, $h^+ = 100$. $-\cdot-$, $Re_\tau = 180$; $-\,-\,-\,-$, $Re_\tau = 550$; ——, $Re_\tau = 1000$.

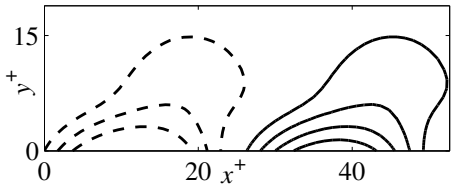

Figure 4. Streamfunction contours of the mode with highest growth rate at $Re_\tau = 550$ for fully developed instability, $\widetilde{K}^+ = 10^4$. Solid and dashed lines correspond to clockwise and counter-clockwise rotation, respectively.

over the others, and appear in the flow overlapped with the background turbulence, as in Jiménez *et al.* (2001) and García-Mayoral & Jiménez (2011*b*). The relevant information for predicting the appearance of Kelvin-Helmholtz rollers is found in the maxima in figure 5(a). This information is condensed in figure 5(b), which shows that the effect of the modulation with $\Phi_{xy}h^+$ is small, and only appears for low values of $\widetilde{K}^+$. García-Mayoral & Jiménez (2011*b*) found a similar relationship between σ^+ and the characteristic length of riblets. In their case, the degradation of drag reduction empirically observed coincided with the sharp transition between the quasi-neutral and the fully developed regimes calculated. This suggested that the model from linear stability could be used to predict the onset of the degradation. In the present case, the sharp transition occurs at $\widetilde{K}^+ \approx 5-10$. Beyond $\widetilde{K}^+ = 5$, the scatter for low values of $\widetilde{K}^+$ discussed above no longer exists. Therefore, the scatter with $\Phi_{xy}h^+$ should have little effect when predicting the onset of the drag degradation. For that reason, the term $\tanh(\Phi_{xy}h^+/y_c^+)$ in expression (15) has little influence on the onset, and can therefore be approximated as its quickly reached limit $\tanh(\Phi_{xy}h^+/y_c^+) \approx 1$. The criterion for the onset is then

$$\widetilde{K}_{MDR}^+ \approx \sqrt{K_x^+ K_y^+} \approx 5-10. \qquad (16)$$

The threshold value $\widetilde{K}_{MDR}^+$ sets a limit for the max-

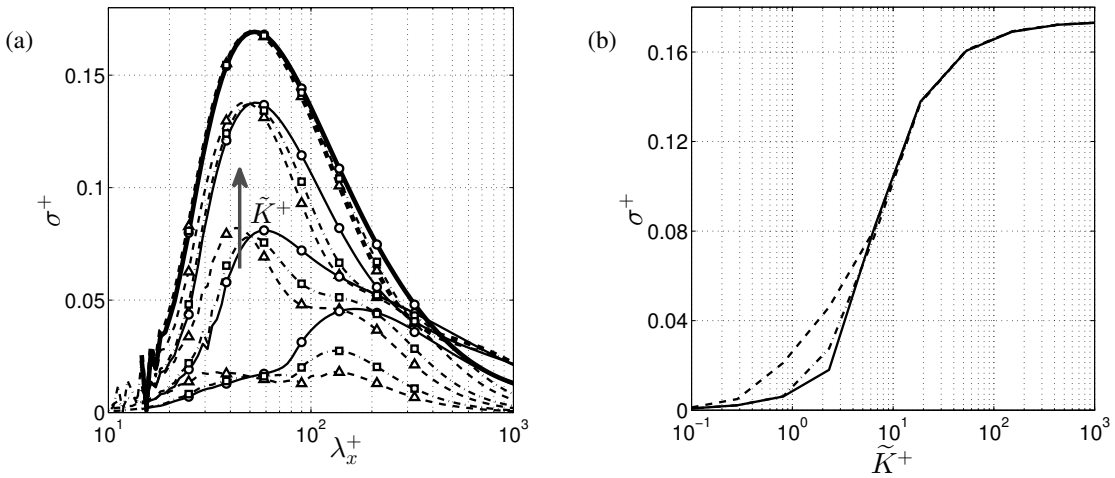

Figure 5. (a) Growth rate $\sigma^+ = \alpha^+ Im(c^+)$ of the most amplified mode as a function of the longitudinal wavelength λ_x. $\widetilde{K}^+ = 10^{[0.36,\ 0.82,\ 1.28,\ 2.20]}$ at $Re_\tau = 550$. ——, $\Phi_x = 10^{-3}$, $h^+ = 10$; - - - -, $\Phi_x = 10^3$, $h^+ = 10$; △, $\Phi_x = 1$, $h^+ = 1$; ○, $\Phi_x = 1$, $h^+ = 100$; -□-, $\Phi_x = 1$, $h^+ = 10$. (b) Maximum growth rate σ^+ as a function of the permeability $\widetilde{K}^+$ at $Re_\tau = 550$. ——$\Phi_x = 10^{-3}$, $h^+ = 1$; - - - -$\Phi_x = 10^3$, $h^+ = 100$; $-\cdot-\Phi_x = 1$, $h^+ = 10$.

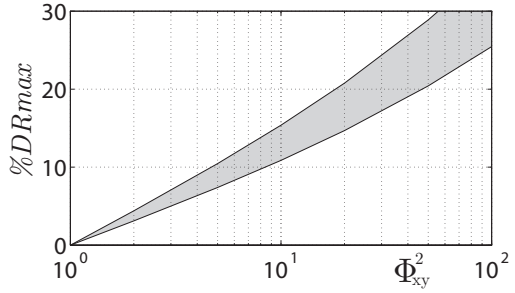

Figure 6. Maximum drag reduction achievable as a function of the anisotropy of the permeable layer, Φ_{xy}^2. The shaded region is bounded by the curves obtained assuming $\widetilde{K}^+_{MDR} = 5$ and $\widetilde{K}^+_{MDR} = 10$.

imum achievable drag reduction. However, it is worth noting that the linear expression for drag reduction (8) was obtained for vanishingly small permeability. Although for riblets the analogous linear behaviour extends until the onset of the Kelvin-Helmholtz mechanism, this may not be the case for the present porous coatings, as other degrading phenomena could appear before reaching $\widetilde{K}^+_{MDR}$. This threshold should therefore be considered with caution, and merely as an upper bound. The present model would need to be validated against experimental or numerical results. For flows over permeable substrates of diverse depth and permeability, it is difficult to find in the literature details on the near-wall structure, but there is at least one case for which Kelvin-Helmholtz rollers are reported at $\widetilde{K}^+ \approx 80$ (Breugem *et al.*, 2006). Although inconclusively, this result would support the validity of our model.

CONCLUSIONS: MAXIMUM DRAG REDUCTION BY PERMEABLE COATINGS

In the present work, we have proposed a simple model to estimate the drag reduction capabilities of permeable coatings. For small permeabilities, the reduction is proportional to the difference between the streamwise and spanwise permeabilities, $DR \propto \sqrt{K_x^+} - \sqrt{K_z^+}$, provided that the coating is sufficiently deep, $h^+ \gg \sqrt{K_x^+}$. However, a Kelvin-Helmholtz instability may arise caused by the presence of the coating. A similar mechanism is responsible for the degradation of performance in riblets of sufficiently large size. The instability generates spanwise rollers near the wall, and consequently degrades the drag reduction. These rollers scale in viscous wall-units and have a height of $y^+ \approx 15$. Using a simple model, this phenomenon can be characterised by a single parameter $\widetilde{K}^+ \approx \sqrt{K_x^+ K_y^+}$.

Combining the predictions of linear drag reduction for small permeability with the onset of the degradation mechanism for larger permeabilities, and assuming that the linear performance persists up to that point, we can estimate the maximum drag reduction that a given permeable layer can achieve. Let us consider a permeable material with a preferential permeability, $K_x^+ > K_y^+ = K_z^+$. The resulting anisotropy ratio, $\Phi_{xy} = \sqrt{K_x/K_y} = \sqrt{K_x/K_z}$, can be used in equations (8) and (16) to obtain an expression for the maximum expected drag reduction,

$$DR_{max} = 0.05 \left(1 - \frac{1}{\Phi_{xy}}\right) \sqrt{\Phi_{xy} \widetilde{K}^+_{MDR}}. \qquad (17)$$

Figure 6 portrays DR_{max} as a function of Φ_{xy}^2, and shows the strong effect of anisotropy on performance. Assuming that the linear behaviour of DR with the permeability ceases at $\widetilde{K}^+_{MDR} = 5$–10, coatings with anisotropy of order $\Phi_{xy} \approx 3$–10, could yield maximum drag reductions of order 15%-25%. This promising result would need to be verified by further studies on this technology.

REFERENCES

Bechert, D.W., Bruse, M., Hage, W., van der Hoeven, J.G.T. & Hoppe, G. 1997 Experiments on drag-reducing surface and their optimization with an adjustable geometry. *J. Fluid Mech.* **338**, 59–87.

Breugem, W.P., Boersma, B.J. & Uittenbogaard, R.E. 2006 The influence of wall permeability on turbulent channel flow. *J. Fluid Mech.* **562**, 35–72.

Brinkman, H.C. 1947 A calculation of the viscous force exerted by a flowing fluid on a dense swarm of particles. *Appl. Sci. Res.* **A1**, 27–34.

Cess, R.D. 1958 A survey of the literature on heat transfer in turbulent tube flow. *Rep. 8-0529-R24. Westinghouse Research*.

Clauser, F.H. 1956 The turbulent boundary layer. *Adv. Appl. Mech* **4**, 1–51.

Darcy, H. 1856 *Les fontaines publiques de la ville de Dijon*. Dalmont.

Drazin, P.G. & Reid, W.H. 1981 *Hydrodynamic stability*. Cambridge University Press.

Finnigan, J. 2000 Turbulence in plant canopies. *Annu. Rev. Fluid Mech.* **32**, 519–571.

García-Mayoral, R. & Jiménez, J. 2011*a* Drag reduction by riblets. *Phil. Trans. R. Soc. A* **369**, 1412–1427.

García-Mayoral, R. & Jiménez, J. 2011*b* Hydrodynamic stability and breakdown of the viscous regime over riblets. *J. Fluid Mech.* **678**, 317–347.

Ghisalberti, M. 2009 Obstructed shear flows: similarities across systems and scales. *J. Fluid Mech.* **641**, 51–61.

Hahn, S., Je, J. & Choi, H. 2002 Direct numerical simulation of turbulent channel flow with permeable walls. *J. Fluid Mech.* **450**, 259–285.

Itoh, M., Tamano, S., Iguchi, R., Yokota, K., Akino, N., Hino, R. & Kubo, S. 2006 Turbulent drag reduction by the seal fur surface. *Phys. Fluids* **18** (6), 065102.

Jiménez, J. 1994 On the structure and control of near wall turbulence. *Phys. Fluids* **6 (2)**, 944–953.

Jiménez, J., Uhlmann, M., Pinelli, A. & Kawahara, G. 2001 Turbulent shear flow over active and passive porous surfaces. *J. Fluid Mech.* **442**, 89–117.

Luchini, P., Manzo, F. & Pozzi, A. 1991 Resistance of a grooved surface to parallel flow and cross-flow. *J. Fluid Mech.* **228**, 87–109.

Neale, G. & Nader, W. 1974 Practical significance of Brinkman's extension of Darcy's law. *The Canadian Journal of Chemical Engineering* **52**, 475–478.

Nikuradse, J. 1933 Laws of flow in rough pipes. *NACA TM 1292*.

Ochoa-Tapia, J.A. & Whitaker, S. 1995 Momentum transfer at the boundary between a porous medium and a homogeneous fluid - I. Theoretical development. *Int. J. Heat Mass Transfer* **38** (14), 2635–2646.

Py, C., De Langre, E. & Moulia, B. 2006 A frequency lock-in mechanism in the interaction between wind and crop canopies. *J. Fluid Mech.* **568**, 425–449.

Rothstein, J.P. 2009 Slip on superhydrophobic surfaces. *Annu. Rev. Fluid Mech.* **42**, 89–109.

Scalo, C., Bodart, J., Lele, S.K. & Joly, L. 2014 Compressible turbulent channel flow with impedance boundary conditions. In *Proceedings of the Summer Program*, pp. 305–314. Center for Turbulence Research.

Schmid, P.J. & Henningson, D.S. 2001 *Stability and transition in shear flows*. Springer.

Squire, H.B. 1933 On the stability for three-dimensional disturbances of viscous fluid flow between parallel walls. *Proc. R. Soc. Lond. A* **142**, 621–628.

Taylor, G.I. 1971 A model for the boundary condition of a porous material. part 1. *J. Fluid Mech.* **49**, 319–326.

Walsh, M.J. & Lindemann, A.M. 1984 Optimization and application of riblets for turbulent drag reduction. *AIAA Paper 84-0347*.